Article

What is the Active Species of Cytochrome P450 during Camphor Hydroxylation? QM/MM Studies of Different Electronic States of Compound I and of Reduced and Oxidized Iron–Oxo Intermediates

Ahmet Altun, Sason Shaik, and Walter Thiel

J. Am. Chem. Soc., **2007**, 129 (29), 8978-8987• DOI: 10.1021/ja066847y • Publication Date (Web): 27 June 2007

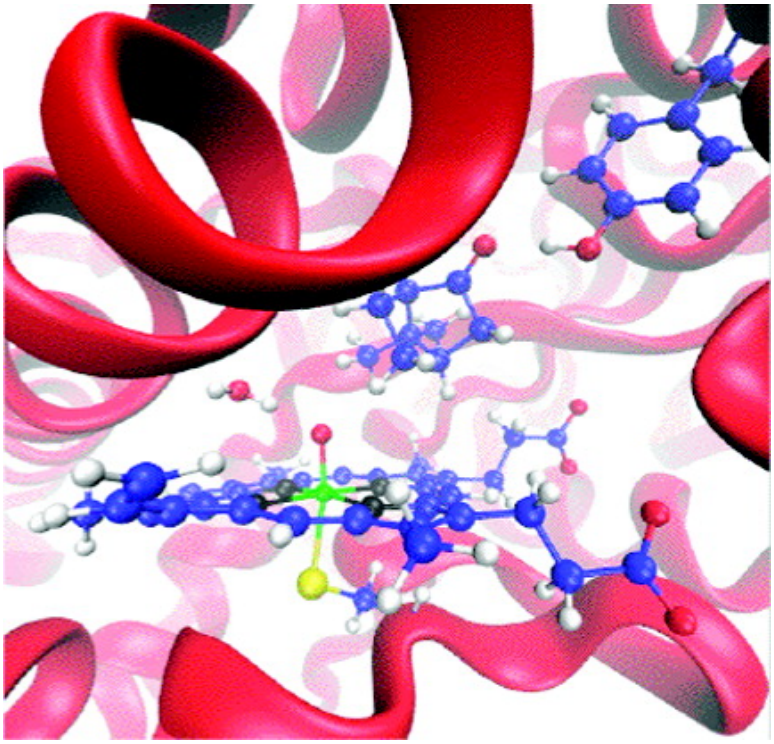

J|A|C|S
ARTICLES
Published on Web 06/27/2007

What is the Active Species of Cytochrome P450 during Camphor Hydroxylation? QM/MM Studies of Different Electronic States of Compound I and of Reduced and Oxidized Iron−Oxo Intermediates

Ahmet Altun,[†] Sason Shaik,[‡] and Walter Thiel*,[†]

Contribution from Max-Planck-Institut für Kohlenforschung, Kaiser-Wilhelm-Platz 1, D-45470 Mülheim an der Ruhr, Germany, and Department of Organic Chemistry and the Lise-Meitner-Minerva Center for Computational Quantum Chemistry, The Hebrew University of Jerusalem, 91904 Jerusalem, Israel

Received September 22, 2006; E-mail: thiel@mpi-muelheim.mpg.de

Abstract: We have investigated C−H hydroxylation of camphor by Compound I (Cpd I) of cytochrome $P450_{cam}$ in different electronic states and by its one-electron reduced and oxidized forms, using QM/MM calculations in the native protein/solvent environment. Cpd I species with five unpaired electrons (pentaradicaloids) are ca. 12 kcal/mol higher in energy than the ground state Cpd I species with three unpaired electrons (triradicaloids). The H-abstraction transition states of pentaradicaloids lie ca. 21 (9) kcal/mol above the triradicaloid (pentaradicaloid) reactants. Hydroxylation via pentaradicaloids is thus facile provided that they can react before relaxing to the ground-state triradicaloids. Excited states of Cpd I with an Fe(V)−oxo moiety lie more than 20 kcal/mol above the triradicaloid ground state in single-point gas-phase calculations, but these electronic configurations are not stable upon including the point-charge protein environment which causes SCF convergence to the triradicaloid ground state. One-electron reduced species (Cpd II) show sluggish reactivity compared with Cpd I in agreement with experimental model studies. One-electron oxidized species are more reactive than Cpd I but seem too high in energy to be accessible. The barriers to hydrogen abstraction for the various forms of Cpd I are generally not affected much by the chosen protonation states of the Asp297 and His355 residues near the propionate side chains of the heme or by the appearance of radical character at Asp297, His355, or the propionates.

I. Introduction

The cytochrome P450 enzymes are hemoproteins that activate regio- and stereoselective C−H bond hydroxylation in several organic substances.[1−3] The putative primary reactive species of these enzymes is an elusive high-valent oxyferryl−porphyrin π-cation species called Compound I (Cpd I, see Scheme 1).[4]

The cryogenic X-ray diffraction and trapping measurements of Schlichting et al.[5] on cytochrome $P450_{cam}$ (CYP101) from the bacterium *Pseudomonas putida* detected electron density that could be tentatively attributed to an oxyferryl species (Cpd I). Such an assignment was questioned by Davydov et al.,[6] whose EPR and ENDOR studies showed that Cpd I of $P450_{cam}$ does not accumulate in a frozen solution at a detection temperature of 200 K and below, indicating that the oxidation of the unactivated C−H bond in camphor has a rate constant exceeding 1000 s^{-1} at ambient temperature. According to these ENDOR measurements,[6] the only detectable intermediate in the catalytic cycle of $P450_{cam}$ after the Fe(III)-hydroperoxy complex (Cpd 0, see Scheme 1) is a Fe(III) bound 5-*exo*-hydroxycamphor species (PC in Scheme 1). The presence of the abstracted hydrogen atom in the alcohol product indicates the involvement of Cpd I in the hydrogen abstraction from camphor.[6]

Cpd I in the thermostable cytochrome P450 CYP119 from *Sulfolobus solfataricus*, which is thought to have a more rigid active site and thus different relative reaction rates than its mesophilic counterpart, has been identified by its characteristic spectral features, and its reactivity toward laurate, a native substrate, was followed and found to be high.[7] Newcomb et al.[8] reported the formation of a P450 Cpd II species (one-electron reduced Cpd I with neutral porphyrin) by peroxynitrite

[†] Max-Planck-Institut für Kohlenforschung.
[‡] The Hebrew University of Jerusalem.

(1) (a) Ortiz de Montellano, P. R., Ed. *Cytochrome P450: Structure, Mechanisms, and Biochemistry*, 2nd ed.; Plenum Presss: New York, 1995. (b) Ortiz de Montellano, P. R., Ed. *Cytochrome P450: Structure, Mechanism, and Biochemistry*, 3rd ed.; Kluwer Academic/Plenum Publishers: New York, 2004.
(2) Denisov, I. G.; Makris, T. M.; Sligar, S. G.; Schlichting, I. *Chem. Rev.* **2005**, *105*, 2253.
(3) Shaik, S.; Kumar, D.; de Visser, S. P.; Altun, A.; Thiel, W. *Chem. Rev.* **2005**, *105*, 2279.
(4) Groves, J. T.; Watanabe, Y. *J. Am. Chem. Soc.* **1988**, *110*, 8443.
(5) Schlichting, I.; Berendzen, J.; Chu, K.; Stock, A. M.; Maves, S. A.; Benson, D. A.; Sweet, R. M.; Ringe, D.; Petsko, G. A.; Sligar, S. G. *Science* **2000**, *287*, 1615.
(6) Davydov, R.; Makris, T. M.; Kofman, V.; Werst, D. E.; Sligar, S. G.; Hoffman, B. M. *J. Am. Chem. Soc.* **2001**, *123*, 1403.
(7) (a) Egawa, T.; Shimada, H.; Ishimura, Y. *Biochem. Biophys. Res. Commun.* **1994**, *201*, 1464. (b) Kellner, D. G.; Hung, S.-C.; Weiss, K. E.; Sligar, S. G. *J. Biol. Chem.* **2002**, *277*, 9641. (c) Spolitak, T.; Dawson, J. H.; Ballou, D. P. *J. Biol. Chem.* **2005**, *280*, 20300.
(8) Newcomb, M.; Zhang, R.; Chandrasena, R. E. P.; Halgrimson, J. A.; Horner, J. H.; Makris, T. M.; Sligar, S. G. *J. Am. Chem. Soc.* **2006**, *128*, 4580.

10.1021/ja066847y CCC: $37.00

Scheme 1. Key Species in the Catalytic Cycle of P450 and Rebound Mechanism for Hydroxylation

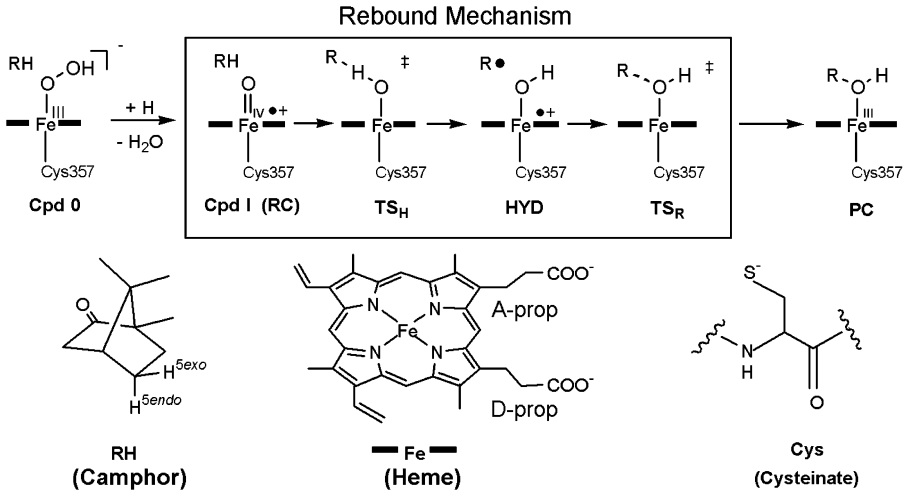

Scheme 2. Orbital Occupancies of Cpd I for (a) Triradicaloid ^{2}A and ^{4}A States as well as (b) Pentaradicaloid ^{4}A and ^{6}A States and (c) Key Porphyrin Orbitals

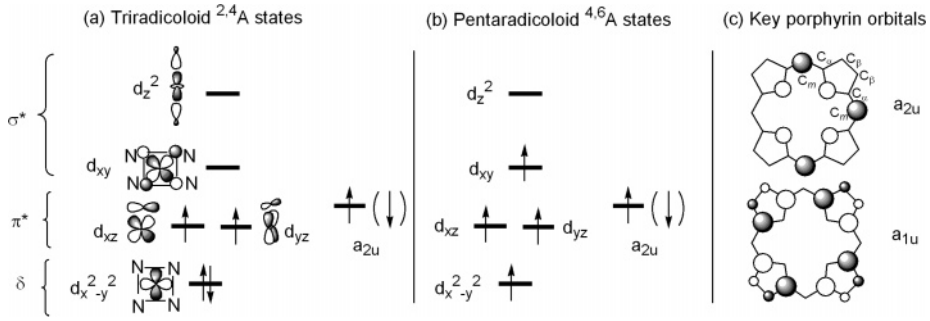

oxidation of the resting state of CYP119 and subsequent conversion of this species by photooxidation in laser flash photolysis experiments to a relatively stable transient, which was assigned to be a Cpd I derivative. The decay of this transient was essentially unchanged in the presence of laurate. Newcomb et al.[8] concluded that Cpd I may thus not be the predominant oxidant, and they proposed that the first-formed oxidant in P450 enzymes could be an iron(V)−oxo species, a high-energy isomer of Cpd I that affects oxidations before it relaxes to the more stable Cpd I species by internal electron rearrangement.[8] However, a previous density functional B3LYP model study[9] has shown that iron(V)−oxo species of Cpd I are high in energy in the gas phase and not stable in a dielectric medium.

Several experimental observations, such as intrinsic kinetic isotope effect measurements[10] and stereochemical scrambling[11] as well as theoretical studies (see ref 3 and references therein) support a two-state rebound mechanism of C−H hydroxylation (see Scheme 1).[12] In the initial rate-limiting H-abstraction reaction of the substrate RH, the reactant complex RC is connected to a hydroxo intermediate radical species HYD by a transition structure TS_H. In the subsequent C−O bond formation step, a ferric−alcohol complex PC is formed via a transition structure TS_R, which has a significant barrier on the quartet surface but a negligible one on the doublet surface[13−15] so that the corresponding transition state TS_R has rarely been located for the doublet.[15]

Cpd I has a virtually degenerate pair of so-called A_{2u} doublet and quartet states (see Schemes 2a and 2c), which give rise to two-state reactivity.[15] Recent B3LYP model and combined quantum mechanical/molecular mechanical (QM/MM) calculations[9,16] show that excited quartet and sextet states of Cpd I generated by promoting one electron from the doubly occupied $\delta(d_{x^2-y^2})$ orbital to the virtual $\sigma^*(d_{xy})$ orbital (see Schemes 2b and 2c) lie ca. 12 kcal/mol above the ground state species. A subsequent B3LYP model study[17] of the corresponding excited-state surfaces indicates that the transition states and intermediates of the rebound mechanism for the allylic hydroxylation of propene are only ca. 5 kcal/mol higher in energy than those on the lowest doublet and quartet surfaces. This calls for a QM/MM study for camphor hydroxylation to assess whether the polarizing environment of protein may reduce this gap further.

The elusiveness of Cpd I in the native cycle of P450 has prompted suggestions for alternative oxidant species. One such alternative is the one-electron reduced Cpd I species (Cpd II).[18−20] Thus, when the catalytic cycle of P450 is shunted by

(9) Ogliaro, F.; de Visser, S. P.; Groves, J. T.; Shaik, S. *Angew. Chem., Int. Ed.* **2001**, *40*, 2874.
(10) Hjelmeland, L. M.; Aronow, L.; Trudell, J. *Biochem. Biophys. Res. Commun.* **1977**, *76*, 541.
(11) Gelb, M. H.; Heimbrook, D. C.; Malkonen, P.; Sligar, S. G. *Biochemistry* **1982**, *21*, 370.
(12) Groves, J. T.; McClusky, G. A. *J. Am. Chem. Soc.* **1976**, *98*, 859.
(13) Ogliaro, F.; Harris, N.; Cohen, S.; Filatov, M.; de Visser, S. P.; Shaik, S. *J. Am. Chem. Soc.* **2000**, *122*, 8977.
(14) Shaik, S.; Cohen, S.; de Visser, S. P.; Sharma, P. K.; Kumar, D.; Kozuch, S.; Ogliaro, F.; Danovich, D. *Eur. J. Inorg. Chem.* **2004**, *35*, 207.
(15) Schöneboom, J. C.; Cohen, S.; Lin, H.; Shaik, S.; Thiel, W. *J. Am. Chem. Soc.* **2004**, *126*, 4017.
(16) Schöneboom, J. C.; Neese, F.; Thiel, W. *J. Am. Chem. Soc.* **2005**, *127*, 5840.
(17) Hirao, H.; Kumar, D.; Thiel, W.; Shaik, S. *J. Am. Chem. Soc.* **2005**, *127*, 13007.
(18) Ogliaro, F.; de Visser, S. P.; Cohen, S.; Sharma, P. K.; Shaik, S. *J. Am. Chem. Soc.* **2002**, *124*, 2806.

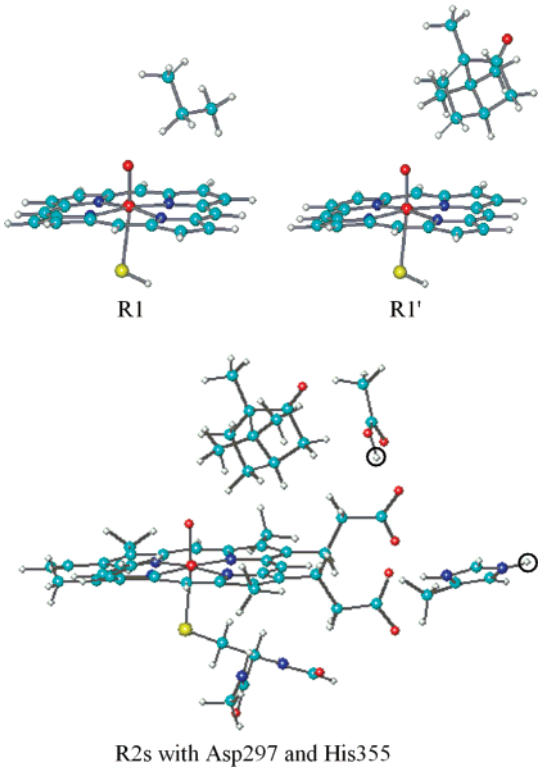

Figure 1. Definition of QM regions.

peroxyacids, EPR spectroscopy detects invariably Cpd II and a protein radical.[21−23] Recent experimental studies on model systems[24−26] imply that Cpd II can carry out both C−H hydroxylations and C═C epoxidations although they are sluggish compared with Cpd I. Cpd II species have been encountered in QM/MM calculations when investigating hydroxylation by Cpd I with deprotonated Asp297 (in QM region) and His355 (see Figure 1).[27−29] In this case, the O−O distance between the A-propionate (A-prop) side chain of heme and Asp297 was found to be very short (ca. 2.2 Å), with one electron being transferred from Asp297 to porphyrin, which thus acquires an almost closed-shell porphyrin configuration. This electronic structure corresponds to Cpd II coupled with an additional unpaired electron shared between the A-prop and Asp297 carboxylate oxygen atoms; in this system, the H-abstraction barrier is 3−4 kcal/mol higher than in its Cpd I analogue.[28]

In this paper, we report QM/MM results for several proposed alternative mechanisms for P450 camphor hydroxylation, involving iron(V)−oxo species, pentaradicaloid Cpd I states, one-electron reduced Cpd I (i.e., Cpd II), and one-electron oxidized Cpd I (Ox-Cpd I). In addition, we address the influence of environmental factors (protonation states of Asp297 and His355).

II. Computational Methodology

A. Setup of the System. The system used in this study includes only the monomer corresponding to the protein chain A and the solvent chain Z of the crystallographic dimer in pdb file 1DZ9.[5] We start from the X-ray structure (1DZ9), add missing hydrogen atoms as well as a 16 Å-thick water layer around the enzyme, and perform a CHARMM[30,31] minimization to remove close contacts keeping the coordinates of heme-Cys357 unit and the outer 8 Å solvent layer fixed. The details of these preparatory force-field calculations are as described in ref 32. This system corresponds to snapX in refs 27 and 28.

B. Protonation States. In all schemes considered (Prot1−Prot3), Asp297 and Glu366 are protonated, on the basis of pK_a values obtained from Poisson−Boltzmann calculations[33] and from the empirical PROPKA procedure[34] as well as inspection of the environment of these residues in the available X-ray structures, compared with the corresponding QM/MM structures (see ref 35 for a detailed discussion). We note that previous QM/MM studies have always assigned Glu366 as being protonated[15,16,27−29,32,35−45] whereas earlier conflicting assignments for Asp297 have now been resolved in favor of the protonated form.[35] Different protonation states may also be considered for histidines. In Prot1, histidines 17, 176, 347, and 391 (21, 62, 337, and 361) are protonated at the ϵ (δ) nitrogen only, while the other histidines are fully protonated at both nitrogen atoms, yielding a net charge of −9e. This protonation scheme is based on previous Poisson−Boltzman electrostatic continuum model calculations.[33] It suffers from artificial long-range electrostatics of the charged surface residues with the QM region when calculating redox potentials.[37] Thus, we also applied a neutral protonation scheme (Prot2)[37] where all histidines and Asp125 are fully protonated. By using still another neutral protonation scheme (Prot3, see Supporting Information), we confirmed that the adopted neutralization scheme has little effect on the computed properties. All results presented in this study refer to Prot1 unless stated otherwise.

C. QM/MM Calculations. The general QM/MM methodology and the protocols adopted in this study have been described extensively elsewhere.[15,16,27,28,32,35−39] In the following, we only address some aspects relevant to the present study.

The QM/MM calculations were performed with the ChemShell package[46] using the TURBOMOLE program[47] for unrestricted open-

(19) Ogliaro, F.; de Visser, S. P.; Shaik, S. *J. Inorg. Biochem.* **2002**, *91*, 554.
(20) Du, P.; Axe, F. U.; Loew, G. H.; Canuto, S.; Zerner, M. C. *J. Am. Chem. Soc.* **1991**, *113*, 8614.
(21) Jung, C. *J. Mol. Recognit.* **2000**, *13*, 325.
(22) Jung, C. *Biochim. Biophys. Acta* **2002**, *1595*, 309.
(23) Meilleur, F.; Contzen, J.; Myles, D. A. A.; Jung, C. *Biochemistry* **2004**, *43*, 8744.
(24) Nam, W.; Lee, H. J.; Oh, S.-Y.; Kim, C.; Jang, H. G. *J. Inorg. Biochem.* **2000**, *80*, 219.
(25) Nam, W.; Park, S.-E.; Kim, I. K.; Lim, M. H.; Hong, J.; Kim, J. *J. Am. Chem. Soc*. **2003**, *125*, 14674.
(26) Kaizer, J.; Klinker, E. J.; Oh, N. Y.; Rohde, J.-U.; Song, W. J.; Stubna, A.; Kim, J.; Münck, E.; Nam, W.; Que, L., Jr. *J. Am. Chem. Soc.* **2004**, *126*, 472.
(27) Altun, A.; Guallar, V.; Friesner, R. A.; Shaik, S.; Thiel, W. *J. Am. Chem. Soc.* **2006**, *128*, 3924.
(28) Altun, A.; Shaik, S.; Thiel, W. *J. Comput. Chem.* **2006**, *27*, 1324.
(29) Guallar, V.; Olsen, B. *J. Inorg. Biochem.* **2006**, *100*, 755.
(30) CHARMM22 force field: MacKerell, A. D., Jr.; Bashford, D.; Bellott, M.; Dunbrack, R. L., Jr.; Evanseck, J. D.; Field, M. J.; Fischer, S.; Gao, J.; Guo, H.; Ha, S.; Joseph-McCarthy, D.; Kuchnir, L.; Kuczera, K.; Lau, F. T. K.; Mattos, C.; Michnick, S.; Ngo, T.; Nguyen, D. T.; Prodhom, B.; Reiher, W. E., III; Roux, B.; Schlenkrich, M.; Smith, J. C.; Stote, R.; Straub, J.; Watanabe, M.; Wiorkiewicz-Kuczera, J.; Yin, D.; Karplus, M. *J. Phys. Chem. B* **1998**, *102*, 3586.
(31) Brooks, B. R.; Burccoleri, R. E.; Olafson, B. D.; States, D. J.; Karplus, M. *J. Comput. Chem*. **1983**, *4*, 187.
(32) Schöneboom, J. C.; Lin, H.; Reuter, N.; Thiel, W.; Cohen, S.; Ogliaro, F.; Shaik, S. *J. Am. Chem. Soc*. **2002**, *124*, 8142.
(33) Lounnas, V.; Wade, R. C. *Biochemistry* **1997**, *36*, 5402.
(34) Li, H.; Robertson, A. D.; Jensen, J. H. *Proteins: Struct. Funct. Bioinf.* **2005**, *61*, 704.
(35) Zheng, J.; Altun, A.; Thiel, W. *J. Comput. Chem.* ASAP article, DOI: 10.1002/jcc.20701.
(36) Schöneboom, J. C.; Thiel, W. *J. Phys. Chem. B* **2004**, *108*, 7468.
(37) Altun, A.; Thiel, W. *J. Phys. Chem. B* **2005**, *109*, 1268.
(38) Lin, H.; Schöneboom, J. C.; Cohen, S.; Shaik, S.; Thiel, W. *J. Phys. Chem. B* **2004**, *108*, 10083.
(39) Zheng, J. J.; Wang, D. Q.; Thiel, W.; Shaik, S. *J. Am. Chem. Soc.* **2006**, *128*, 13204.
(40) Guallar, V.; Baik, M.; Lippard, S. J.; Friesner, R. A. *Proc. Natl. Acad. Sci. U.S.A.* **2003**, *100*, 6998.
(41) Guallar, V.; Friesner, R. A. *J. Am. Chem. Soc.* **2004**, *126*, 8501.
(42) Bathelt, C. M.; Zurek, J. L.; Mulholland, A. J.; Harvey, J. N. *J. Am. Chem. Soc.* **2005**, *127*, 12900.
(43) Zurek, J.; Foloppe, N.; Harvey, J. N.; Mulholland, A. J. *Org. Biomol. Chem.* **2006**, *4*, 3931.
(44) Harvey, J. N.; Bathelt, C. M.; Mulholland, A. J. *J. Comput. Chem.* **2006**, *27*, 1352.
(45) Swart, M.; Groenhof, A. R.; Ehlers, A. W.; Lammertsma, K. *Chem. Phys. Lett.* **2005**, *403*, 35.

shell density functional theory (DFT) calculations with the B3LYP functional[48] and the DL-POLY program[49] for MM calculations with the CHARMM22 force field.[30] The HDLC optimizer[50] in ChemShell was employed for geometry optimizations. A rational function optimizer with the Powell update (P-RFO) for an explicit Hessian[50] was used in transition-state (TS) optimizations. An electronic embedding scheme[51] was applied to include the polarizing effect of the enzyme environment on the QM region. Hydrogen link atoms[52] were used at the QM/MM boundary along with the charge shift model.[53] No cutoffs were introduced for the nonbonding MM and QM/MM interactions.

Previous experience[28,32,37] shows that the smallest possible proximal ligand representation of SH in the QM region yields QM/MM results analogous to those with more extended representations. We employed a number of QM regions (see Figure 1), which comprised the following sets of atoms: (i) R1 (51 QM atoms): Iron−oxo−porphyrin (without heme side chains), $C^4HC^5H_2C^6H_2$ part of camphor which corresponds to propane in gas-phase calculations, and sulfur atom of coordinating Cys357. (ii) R1′ (67 QM atoms): R1 region with full camphor. (iii) The influence of the protonation states of Asp297 and His355 was investigated by including these residues in the R2s region (120 QM atoms) that contains iron−oxo−porphyrin (including all heme side chains), full camphor, Cys357, CO group of Leu356, and NH−C^{α}H unit of Leu358. In this case, Asp297 and His355 were represented as follows: CH_3COOH (protonated Asp297), CH_3COO^- (deprotonated Asp297), methyl-substituted imidazole (protonated His355), and methyl-substituted imidazolate (deprotonated His355). The labels Asp and Aspp (Hsd and Hsp) after the R2s abbreviation denote the inclusion of deprotonated and protonated Asp297 (His355) in the QM region, respectively. The hydrogen atoms, which are added or removed from the system, are marked by circles in Figure 1.

The R1 region was used in extensive QM/MM optimizations while R1′ was utilized only for single-point calculations. QM/MM geometry optimizations were also performed using the large R2s region with Asp297 and/or His355 for some cases. TS optimizations were not performed for the calculations with extended R2s QM regions, instead the O−H^{5exo} distance in TS_H was refined with an increment of 0.01 Å.

Three basis sets were employed. B1 and B2 describe iron by a small-core effective core potential (ECP) together with the associated double-ζ quality LACVP basis,[54] but differ for the other atoms. (i) B1: 6-31G[55] on all other atoms. (ii) B2: 6-31+G*[55] for the six atoms coordinated to iron, and C^5 as well as O of camphor; 6-31++G**[55] for H^{5exo} of camphor; 6-31G for the remaining atoms. (iii) B2W: Wachters all-electron basis set in the contraction [8s6p4d2f][56] for Fe; otherwise B2. B1 is for geometry optimization whereas B2 and B2W are for single-point calculations.

Throughout this study, the QM level employed in a particular QM/MM calculation is denoted in the form QM region/basis set, e.g., R1/B1, R1′/B2W, etc. The QM/MM optimizations included all residues and water molecules that have atoms within a distance of 4 (6) Å around any atom of the iron−oxo−porphyrin−Cys357 complex and the substrate camphor for R1/B1 (R2s/B1 with Asp297 and/or His355 in the QM region), that is, 435 (863) atoms (see Supporting Information for the list of optimized residues). The oxidation state of iron is specified after the symbol of a given species in parentheses.

III. Results

A. The Effect of QM Regions and Basis Sets. The previous QM/MM calculations on H-abstraction by Cpd I show that partial inclusion of camphor in the QM region (R1) results in an underestimation of the H-abstraction barrier by 2−3 kcal/mol compared with QM regions that include camphor completely (R1′).[27,28] Such a difference is not seen in the gas phase.[27,28] It probably arises from the stretching of the H-bond between camphor and Tyr96 in TS_H compared with RC and HYD, whose energetic effect is not captured by the MM force field. This error in the R1 QM/MM barrier is systematic and occurs also for Cpd II and Ox-Cpd I to some extent (1−3 kcal/mol) depending on the O−H^{5exo} distance and thus the amount of H-bond stretching between camphor and Tyr96 (see below).

Going from basis set B1 to B2, the relative QM/MM energies of TS_H and HYD(IV) with respect to RC are almost unchanged whereas those of HYD(III) and PC(III) are lowered by ca. 4 kcal/mol. Going from B2 to B2W, the relative QM/MM energies of TS_H/HYD(III) {HYD(IV)} are increased {decreased} by ca. 2/4 {3} kcal/mol with respect to RC. Thus, whereas B1 and B2W results are analogous for HYD(III), B1 underestimates {overestimates} B2W energies for TS_H {HYD(IV)} by ca. 2 {3} kcal/mol. These rather uniform basis set effects are found not only for Cpd I but also for its redox species (see Supporting Information). This allows us to compare the behavior of Cpd I, Cpd II, and Ox-Cpd I in the hydroxylation reaction at the R1/B1 level in the following. Higher-level single-point QM/MM results on R1/B1 geometries are only presented for some selected spin states.

B. Hydroxylation by Triradicaloid Cpd I. Recent QM/MM studies on the H-abstraction reaction identified a catalytic water molecule (w903 in 1DZ9 pdb structure) that lowers the computed barrier by 4 kcal/mol.[27,28] Since this water molecule was not present in our previous QM/MM calculations on two-state reactivity in $P450_{cam}$,[15] we have now reinvestigated the complete two-state rebound mechanism using the new setup (snapX)[27,28] with the catalytic water molecule being H-bonded to the oxo ligand. The resulting energy profiles are shown in Figure 2. Detailed geometrical data for each species during the rebound mechanism can be found in Supporting Information. Individual (Fe and O), average (N), and group (SH, camphor, and porphyrin) spin densities are given in Table 1.

The present results confirm that the two-state reactivity paradigm for P450 hydroxylation remains valid also in the presence of the catalytic water molecule: w903 lowers the H-abstraction barrier/endothermicity by ca. 4/6 kcal/mol both

(46) (a) Sherwood, P.; de Vries, A. H.; Guest, M. F.; Schreckenbach, G.; Catlow, C. R. A.; French, S. A.; Sokol, A. A.; Bromley, S. T.; Thiel, W.; Turner, A. J.; Billeter, S.; Terstegen, F.; Thiel, S.; Kendrick, J.; Rogers, S. C.; Casci, J.; Watson, M.; King, F.; Karlsen, E.; Sjovoll, M.; Fahmi, A.; Schäfer, A.; Lennartz, C. *J. Mol. Struc. (THEOCHEM)* **2003**, *632*, 1. (b) ChemShell is a modular QM/MM program based on the TCL interpreter and developed in the European QUASI project under the coordination of P. Sherwood. See: http://www.cse.clrc.ac.uk/qcg/chemshell.
(47) (a) Ahlrichs, R.; Bär, M.; Häser, M.; Horn, H.; Kölmel, C. *Chem. Phys. Lett.* **1989**, *162*, 165. (b) Ahlrichs, R.; Bär, M.; Baron, H.-P.; Bauernschmitt, R.; Böcker, S.; Ehrig, M.; Eichkorn, K.; Elliot, S.; Furche, F.; Häser, M.; Horn, H.; Hättig, C.; Huber, C.; Huniar, U.; Kattanneck, M.; Köhn, A.; Kölmel, C.; Kollwitz, M.; May, K.; Ochsenfeld, C.; Öhm, H.; Schäfer, A.; Schneider, U.; Treutler, O.; v. Arnim, M.; Weigend, F.; Weis, P.; Weiss, H. TURBOMOLE 5.5, University of Karlsruhe, 2002.
(48) (a) Becke, A. D. *Phys. Rev. A* **1988**, *38*, 3098. (b) Lee, C.; Yang, W.; Parr, R. G. *Phys. Rev. B* **1988**, *37*, 785. (c) Becke, A. D. *J. Chem. Phys*. **1993**, *98*, 5648.
(49) Smith, W.; Forester, T. *J. Mol. Graph.* **1996**, *14*, 136.
(50) Billeter, S. R.; Turner, A. J.; Thiel, W. *Phys. Chem. Chem. Phys*. **2000**, *2*, 2177.
(51) Bakowies, D.; Thiel, W. *J. Phys. Chem*. **1996**, *100*, 10580.
(52) Antes, I.; Thiel, W. *Hybrid Quantum Mechanical and Molecular Mechanical Methods*; Gao, J., Ed.; ACS Symposium Series 712, American Chemical Society: Washington, DC, 1998; pp 50−65.
(53) de Vries, A. H.; Sherwood, P.; Collins, S. J.; Rigby, A. M.; Rigutto, M.; Kramer, G. J. *J. Phys. Chem. B* **1999**, *103*, 6133.
(54) Hay, J. P.; Wadt, W. R. *J. Chem. Phys*. **1985**, *82*, 299.
(55) (a) Ditchfield, R.; Hehre, W. J.; Pople, J. A. *J. Chem. Phys*. **1971**, *54*, 724. (b) Hehre, W. J.; Ditchfield, R.; Pople, J. A. *J. Chem. Phys*. **1972**, *56*, 2257. (c) Hariharan, P. C.; Pople, J. A. *Theor. Chim. Acta* **1973**, *28*, 213. (d) Clark, T.; Chandrasekhar, J.; Spitznagel, G. W.; Schleyer, P. v. R. *J. Comput. Chem*. **1983**, *4*, 294.
(56) (a) Wachters, A. J. H. *J. Chem. Phys.* **1970**, *52*, 1033. (b) Hay, P. J. *J. Chem. Phys.* **1977**, *66*, 4377. (c) Bauschlicher, C. W., Jr.; Langhoff, S. R.; Barnes, L. A. *J. Chem. Phys.* **1989**, *91*, 2399.

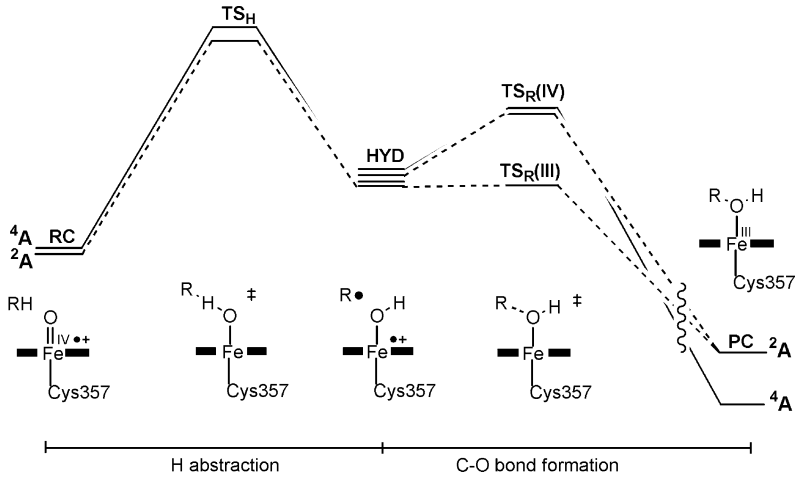

		RC	TS_H	HYD(III)/HYD(IV)	TS_R(III)/TS_R(IV)	PC
^{2}A	B1	0.0	15.8	9.0/11.7	9.2/13.8	-40.3
	B2W	0.0	17.8	8.0/7.7	8.0/9.9	-45.3
^{4}A	B1	0.1	17.1	10.1/12.5	- /13.9	-45.6
	B2W	0.3	19.1	9.2/8.5	- /10.3	-51.2

Figure 2. R1/B1 QM/MM energy profiles (kcal/mol) for the rebound mechanism. Solid (dashed) lines refer to the quartet (doublet) state. The oxidation state of iron is indicated in parentheses. Numerical values for R1/B1 and R1/B2W relative energies are given at R1/B1-optimized geometries.

Table 1. R1/B1 Mulliken Spin Densities of the Species during Rebound Mechanism by Cpd I

		Fe	O	SH	N	Cam	Porp
^{2}A	RC(IV)	1.29	0.83	−0.23	−0.17	0.01	−0.90
	TS_H(III)	1.07	0.52	−0.21	−0.17	0.46	−0.84
	HYD(III)	1.04	0.11	−0.16	−0.18	0.89	−0.87
	HYD(IV)	1.96	0.20	−0.13	−0.04	−0.91	−0.12
	TS_R(III)	1.05	0.05	−0.13	−0.15	0.78	−0.75
	TS_R(IV)	1.76	0.23	−0.10	−0.03	−0.80	−0.09
	PC(III)	1.39	0.00	−0.17	−0.06	0.00	−0.21
^{4}A	RC(IV)	1.15	0.88	0.19	0.16	0.01	0.77
	TS_H(III)	0.93	0.59	0.19	0.15	0.53	0.77
	HYD(III)	0.90	0.19	0.15	0.16	0.95	0.81
	HYD(IV)	2.03	0.25	−0.10	−0.04	0.94	−0.12
	TS_R(IV)	2.32	0.06	−0.04	−0.05	0.79	−0.13
	PC(III)	2.61	0.00	0.35	−0.01	0.00	0.04
^{4}A′	RC(IV)	3.21	0.65	−0.28	−0.09	0.00	−0.59
	TS_H(IV)	3.92	0.07	−0.40	−0.03	−0.38	−0.20
	HYD(IV)	4.07	0.33	−0.44	−0.01	−0.89	−0.07
^{6}A	RC(IV)	3.10	0.67	0.04	0.25	0.01	1.19
	TS_H(IV)	3.85	−0.02	0.47	0.22	−0.32	1.03
	HYD(IV)	4.01	0.32	0.50	0.23	−0.89	1.06

in the quartet[27,28] and the doublet state but does not affect the rebound step much. The H-abstraction step thus remains rate-determining, and the rebound is essentially barrierless in the doublet Fe(III) species but encounters a small non-negligible barrier in the quartet state.

The potential energy surface (PES) for rebound (C−O bond formation) is very flat, and it is thus very difficult to locate TS_R structures precisely. Those found presently [^2TS_R(III), ^2TS_R(IV) and ^4TS_R(IV)] with w903 near the oxo ligand are very similar to previous approximate structures[15] without w903 near the oxo ligand, both geometrically and energetically (relative to HYD). This emphasizes that the presence of w903 near the oxo ligand does not influence the C−O bond formation step significantly. In our previous study,[15] we reported a ^4TS_R(III) structure, which lies ca. 4 kcal/mol above TS_H. Presently, we could not locate such a ^4TS_R(III) structure as H^{5exo} is transferred back to camphor during the PES scan before a TS structure connecting ^{4}HYD(III) to PC is encountered. Hence, in the quartet state, there seems to be only one accessible rebound channel via ^4TS_R(IV) in the enzyme. This however does not rule out the population of the ^{4}HYD(III) intermediate, which will increase the lifetime of the radical on the quartet surface.

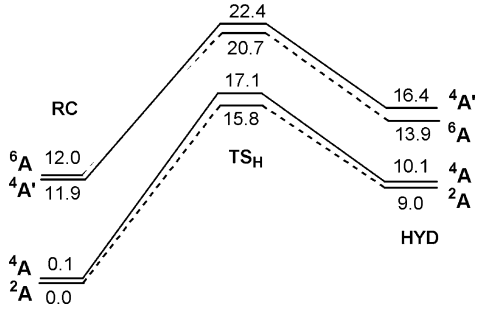

Figure 3. R1/B1 QM/MM energy profile (kcal/mol) for H-abstraction by triradicaloid (^{2}A, ^{4}A) and pentaradicaloid (^{4}A′, ^{6}A) Cpd I.

Considering basis set effects, we performed additional calculations on the H-abstraction step with the following larger B3 basis: Wachters all-electron basis set[56] in the contraction [8s6p4d2f] for iron as in B2W; TZVP[57] for the six atoms coordinated to iron and for C[5]; TZVPP[57] for H^{5exo}; SV[58] for the remaining atoms. R1/B3 QM/MM optimizations yield TS_H(III)/HYD(III)/HYD(IV) structures that lie 17.8/6.4/4.6 kcal/mol (^{2}A) and 19.2/7.6/5.2 kcal/mol (^{4}A) above RC(IV). Hence, the R1/B3 and R1/B2W barriers are essentially identical (see Figure 3) whereas the HYD intermediates become somewhat more stable with the larger basis B3. Contrary to the R1/B1 and R1/B2W cases, the R1/B3 calculations also converge for the TS_H(IV) species which are found at 16.3 (^{2}A) and 19.3 (^{4}A) kcal/mol, i.e., close to the TS_H(III) species, indicating that the Fe(IV) surface may already become accessible during the H-abstraction step (see Supporting Information for B3 spin densities and geometry parameters).

(57) (a) Ahlrichs, R.; May, K. *Phys. Chem. Chem. Phys.* **2000**, *2*, 943. (b) Schäfer, A.; Huber, C.; Ahlrichs, R. *J. Chem. Phys.* **1994**, *100*, 5829.
(58) Schäfer, A.; Horn, H.; Ahlrichs, R. *J. Chem. Phys.* **1992**, *97*, 2571.

C. H-Abstraction by Pentaradicaloid Cpd I and Other Excited States. The H-abstraction energy profiles for the pentaradicaloid states with five unpaired electrons (^{6}A and ^{4}A′; the prime distinguishes tri- and pentaradicaloid ^{4}A states, see Scheme 2) are given in Figure 3 and compared to those for the triradicaloid states. The RC pentaradicaloids (Cpd I) are 12 kcal/mol higher in energy than the triradicaloids at R1/B1 and single-point R1′/B1 levels. The TS_H/HYD pentaradicaloids lie 22.4/16.4 (23.5/16.6) kcal/mol [^{4}A′] and 20.7/13.9 (21.5/14.1) kcal/mol [^{6}A] above the doublet ground state at the R1/B1 level. The R1 and R1′ results are similar as the H-bond between camphor and Tyr96 is less stretched than in the triradicaloids (see below). As previously found in the gas phase,[17] the transition states of pentaradicaloid states are ca. 5 kcal/mol higher in energy than those of the triradicaloids.

In the pentaradicaloids, iron is displaced out of the heme plane to the distal side by ca. 0.1 Å for RC and by 0.2−0.3 Å for TS and HYD due to the occupation of the σ^*_{xy} orbital. There is more electron density on the FeO unit of pentaradicaloids compared with triradicaloids (see Table 1), and therefore TS_H occurs relatively early, as can be seen from O−H^{5exo} distances of 1.20/1.19/1.29/1.36 Å for ^{2}A/^{4}A/^{4}A′/^{6}A. The partial population of the $\sigma^*_{z^2}$ orbital [σ^*(Fe−S) character] results in the elongation of Fe−S bond by ca. 0.3 Å in TS_H and HYD (see Supporting Information).

In view of the recent claim[8] that Fe(V)−oxo species may act as primary oxidant in P450 hydroxylation, we have attempted to calculate such states, with very limited success. For example, at the optimized R1/B1 QM/MM geometry of quartet Cpd I, a gas-phase R1/B1 QM calculation yields a quartet Fe(V)−oxo species (spin densities: Fe, 2.17e; O, 1.16e; SH, −0.21e; porphyrin, −0.14e) which lies 23.7 kcal/mol above the doublet ground state, analogous to a previous gas-phase result of 26.6 kcal/mol.[9] However, when including the point charges from the MM environment, the DFT calculation converged during the self-consistent-field (SCF) procedure no longer to the Fe(V)−oxo solution but to the usual Fe(IV)−oxo ground state. This behavior was encountered in several attempts (different geometries, different convergence strategies) and also in previous work when a dielectric medium was included in gas-phase model calculations.[9] It thus appears that Fe(V)−oxo species of Cpd I are not stable in a protein/solvent environment, even less so than in the gas phase. The lack of SCF convergence indicates that the corresponding electronic configuration is less favorable, but it does not prove the nonexistence of such excited-state species, of course. In an attempt to estimate the energy of such states, we have carried out time-dependent (TD) DFT calculations at the R1/B1 QM/MM geometry of quartet Cpd I and TS_H starting from the corresponding QM/MM density matrices (B3LYP). In the case of Cpd I, the ninth and tenth excited states at 1.69 and 1.79 eV (39.0 and 41.3 kcal/mol), respectively, are the first ones that originate mainly from transitions out of the $d_{x^2-y^2}$ orbital at iron and may thus be regarded as Fe(V) states (all lower excited quartet states involve excitations from porphyrin or sulfur orbitals). Likewise, in the case of TS_H, the first excited quartet states with significant Fe(V) character are found at 1.62 and 1.86 eV (37.6 and 42.9 kcal/mol). Similar results are obtained from analogous single-point TDDFT calculations in the gas phase or with a large basis. For doublet Cpd I and TS_H, the first excited states with appreciable Fe(V) character lie even higher (above 2 eV or 46 kcal/mol). Our current DFT and TDDFT results thus do not support an involvement of Fe(V)−oxo species in P450 hydroxylation.

Scheme 3. Orbital Occupancies in Cpd II

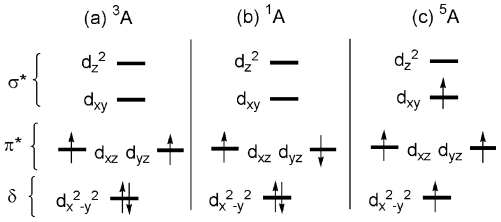

Concerning other excited states of Cpd I, we obtained convergence for a doublet configuration (^{2}A) with a singly occupied a_{2u} porphyrin orbital and two electrons of opposite spin in the π^* orbitals of the FeO moiety. This doublet lies 9.4 kcal/mol above the doublet ground state and has an H-abstraction barrier of ca. 10 kcal/mol (i.e., TS_H at 19 kcal/mol relative to the doublet ground state). We also got convergence for two excited sextet configurations (^{6}A), one with five unpaired electrons on the FeO unit and the other one with four unpaired electrons on the FeO unit and the fifth one in a predominantly porphyrin a_{2u} orbital (with some sulfur p admixture). These two sextets lie ca. 25/13 kcal/mol above the doublet ground state/lowest sextet state (see Supporting Information) and have H-abstraction barriers of only 4−5 kcal/mol (i.e., TS_H at 30 kcal/mol relative to the doublet ground state).

In summary, the pentaradicaloid and other excited Cpd I species that have been characterized by QM/MM calculations can easily abstract hydrogen from camphor, with barriers of typically 10 kcal/mol or less. However, on an absolute scale relative to the doublet ground state of Cpd I, the calculated (R1/B1) energies of the transition state (TS_H) are of the order of 20 kcal/mol or more and thus higher in energy than those for the ground-state reaction (see Figure 3). It is unclear whether such excited Cpd I species can be formed in the enzyme, and if so, whether they can affect oxidation before relaxing to the lower-energy states. Our calculations provide no evidence for Fe(V)−oxo species of Cpd I that have been proposed to act in this manner.[8]

D. H-Abstraction Reaction by Cpd II. Upon reduction of Cpd I, the singly occupied a_{2u} porphyrin orbital is filled, yielding an essentially closed-shell porphyrin. The orbital occupancies in the low-lying diradicaloid states (^{3}A and ^{1}A) and the tetraradicaloid quintet states (^{5}A) of the one-electron reduced species of Cpd I (Cpd II) are shown in Scheme 3. The R1/B1 energy order is ^{3}A < ^{1}A < ^{5}A (0 < 8.7 < 11.8 kcal/mol) for Cpd II (see Figure 4).

For the triplet ground state (^{3}A) of Cpd II, the R1/B1 barrier/endothermicity is 20.6/13.4 kcal/mol and thus ca. 5/4 kcal/mol higher than for the doublet ground state of Cpd I (15.8/9.0 kcal/mol). In the open-shell singlet (^{1}A) and the quintet (^{5}A) state, the H-abstraction barriers are computed to be 14.2 and 22.1 kcal/mol, respectively, resulting in transition state energies (TS_H) of ca. 23 and 34 kcal/mol relative to the triplet ground state. Thus, *C−H hydroxylation by Cpd II of P450$_{cam}$ is sluggish compared with Cpd I, in agreement with previous experimental model studies.*[24−26] Therefore, we have not investigated the C−O bond formation step of the rebound mechanism by Cpd II.

Table 2 lists selected Mulliken spin densities for the relevant species. As the H-abstraction proceeds, one electron is gradually

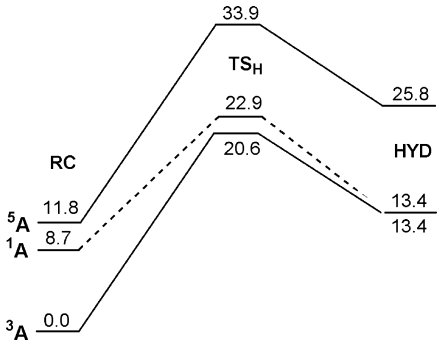

Figure 4. R1/B1 QM/MM energy profile (kcal/mol) for H-abstraction by Cpd II.

Table 2. R1/B1 Mulliken Spin Densities of the Species during H-Abstraction by Cpd II

		Fe	O	SH	Cam	Porp
^{3}A	RC(IV)	1.28	0.84	−0.02	0.01	−0.07
	TS_H(III)	1.03	0.53	−0.02	0.53	−0.06
	HYD(III)	0.99	0.13	−0.01	0.96	−0.07
^{1}A	RC(IV)	0.61	−0.58	0.02	0.01	−0.06
	TS_H(III)	0.94	−0.36	−0.02	−0.49	−0.07
	HYD(III)	0.97	0.08	−0.01	−0.97	−0.07
^{5}A	RC(IV)	3.18	0.64	−0.10	0.00	0.27
	TS_H(III)	2.98	0.41	−0.10	0.52	0.20
	HYD(III)	2.91	0.03	−0.07	0.97	0.17

transferred from camphor to the FeO moiety, so that the spin density at camphor changes from 0 initially (closed-shell) to ca. 1e (^{3}A, ^{5}A) or −1e (^{1}A) in the hydroxo intermediate.

When full camphor is included in the QM region, the barrier/endothermicity on the ^{3}A surface (R1/B1: 20.6/13.4 kcal/mol) becomes 21.9/13.5 (21.8/9.9) {24.2/12.9} kcal/mol at the R1′/B1 (R1′/B2) {R1′/B2W} level (single-point calculations). Hence, the effects of including full camphor in the QM region and of basis set improvement are analogous for Cpd I and Cpd II (see Section III.A and III.B).

Considering the effect of the protonation state of Asp297 and His355, we previously found that R2sAsp/B1 and R2sAspHsd/B1 calculations on the quartet state both yield 23.6/13.3 kcal/mol for the barrier/endothermicity. The structures with deprotonated Asp297 in the QM region correspond to triplet state Cpd II ferromagnetically coupled with an electron located on the A-prop and Asp297 carboxylates. Comparing with the R1′/B1 result of 21.9/13.5 kcal/mol (see above), it is obvious that Cpd II reactivity is not affected much by the local environment of propionate.

For the sake of completeness, we note that we have also studied the closed-shell singlet (^1A_c) and an excited quintet (^{5}A′: singly occupied orbitals d_{xz}, d_{yz}, a_{1u}, a_{2u}) of Cpd II. These states and the corresponding transition states are very high in energy and thus mechanistically irrelevant (see Supporting Information for details).

E. Hydroxylation by Ox-Cpd I. In view of the current interest in iron complexes with oxidation states higher than Fe(IV), we looked at the oxidized form of Cpd I. Test calculations with different orbital occupation patterns show that the most stable oxidized Cpd I species are obtained by removing an electron from the highest doubly occupied porphyrin π orbital. Thus, the heme framework does not support iron in oxidation states higher than 4, since the oxidation equivalent ends on the porphyrin. This gives rise to tetraradicaloid species

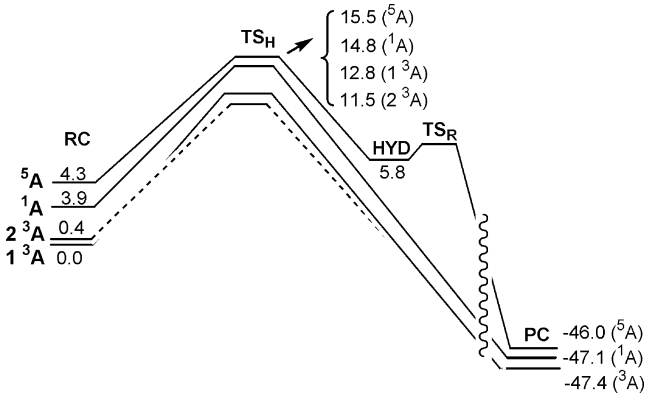

Figure 5. R1/B1 QM/MM energy profile (kcal/mol) for the hydroxylation reaction by Ox-Cpd I.

Scheme 4. Orbital Occupancies in Ox-Cpd I

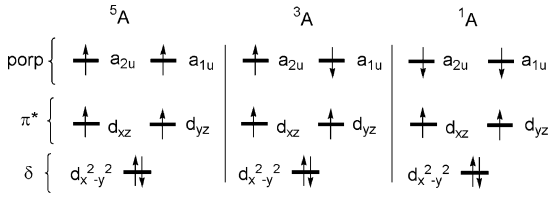

Table 3. R1/B1 Mulliken Spin Densities of the Species during Hydroxylation Reaction by Ox-Cpd I

		Fe	O	SH	Cam	Porp
1 ^{3}A	RC(IV)	1.08	0.94	0.24	0.01	−0.28
	TS_H (III)	0.94	0.63	0.18	0.46	−0.20
	PC(III)	1.25	0.00	−0.16	0.00	0.90
2 ^{3}A	RC(IV)	1.24	0.87	−0.28	0.01	0.16
	TS_H (III)	1.06	0.55	−0.24	0.36	0.27
^{1}A	RC(IV)	1.23	0.87	−0.45	0.01	−1.65
	TS_H (III)	1.10	0.53	−0.34	0.29	−1.57
	PC(III)	1.19	−0.01	−0.12	0.00	−1.06
^{5}A	RC(IV)	1.09	0.93	0.36	0.01	1.60
	TS_H(IV)	1.41	0.76	0.30	0.44	1.09
	HYD(IV)	1.99	0.29	−0.01	0.87	0.87
	HYD(III)	0.88	0.23	0.33	0.94	1.62
	PC(IV)	3.98	0.01	0.38	0.00	−0.37

with four unpaired electrons, two in the π* orbitals of the FeO unit (d_{xz}, d_{yz}) and two in the highest porphyrin π orbitals (a_{2u}, a_{1u}). It should be stressed that the labels (in parentheses) are just short-hand notations which, for example, do not reflect the mixing between the a_{2u} and a_{1u} porphyrin orbitals and the admixture of sulfur p orbitals that is invariably found in the unsymmetrical geometries considered presently. With this proviso, Scheme 4 indicates the lowest-energy electron configurations for the quintet, triplet, and singlet states of the tetraradicaloid Ox-Cpd I species.

In these configurations, the electrons in the π*(FeO) orbitals always have parallel spin while those in the porphyrin orbitals assume different spin orientations. According to the R1/B1 QM/MM calculations, there are two almost degenerate triplet states with porphyrin/SH spin densities of −0.28e/0.24e (1 ^{3}A) and 0.16e/−0.28e (2 ^{3}A), and all four states lie within 5 kcal/mol: 1 ^{3}A ≤ 2 ^{3}A < ^{5}A ≤ ^{1}A (1 ^{3}A and 2 ^{3}A have opposite spins in the two porphyrin orbitals). Figure 5 shows the R1/B1 QM/MM energy profiles computed for these states, and Table 3 lists the R1/B1 Mulliken spin densities of the relevant species.

The computed barriers are rather small for all four states (ca. 11−13 kcal/mol), and the corresponding transition states lie

11.5−15.5 kcal/mol above the triplet ground state of Ox-Cpd I. A hydroxo intermediate (HYD) could be located only in the case of the quintet state (Figure 5). QM/MM energy scans for H-abstraction led to HYD-like structures (about 10 kcal/mol below TS_H) also in the case of the triplet and singlet states, which however relaxed directly to the product complex (PC) upon unconstrained optimization.

As might have been expected from the higher effective oxidation state, the two lowest triplet states of Ox-Cpd I are stronger hydroxylation agents than Cpd I because the corresponding barriers are lower by ca. 4 kcal/mol. Both states give the same hydroxylation product, a hexacoordinated complex in which one electron has been transferred from a porphyrin π orbital to a π*(FeO) orbital yielding a diradicaloid triplet product. Hydroxylation of the open-shell singlet (^{1}A) also generates a hexacoordinated product complex, with a similar electron redistribution as in the triplet case. Hydroxylation of the quintet (^{5}A) follows a somewhat different course: The initial electron transfer on the way toward the transition state (RC → TS_H) occurs from camphor to porphyrin (rather than to the FeO unit), there is a HYD intermediate (with two electromeric minima, HYD(IV) being more stable than HYD(III) by 5.4 kcal/mol), and the product complex has a pentacoordinated iron center. These differences should however not distract from the main finding that all four states of Ox-Cpd I have low barriers and should thus be excellent hydroxylation agents.

For the sake of completeness we mention again that we have also investigated several other states of Ox-Cpd I (open-shell singlets ^{1}A′ and ^{1}A″, closed-shell singlet ^1A_c) which turned out to be higher in energy and thus less relevant (see Supporting Information). We have also targeted Fe(V) variants of Ox-Cpd I and managed to converge a corresponding ^{5}A state with one electron removed from the iron $d_{x^2-y^2}$ orbital rather than from a porphyrin orbital (spin density: Fe, 2.15e; O, 1.11e; SL, −0.05e; porp, 0.78e; cam, 0.02e). This Fe(V) species was ca. 19 kcal/mol above the lowest Ox-Cpd I quintet (see Figure 5) in a single-point calculation and could not be optimized due to SCF convergence problems (see Section III. C).

We conclude this section with some technical remarks: The relative spin state energies agree in R1 and R1′ calculations on Ox-Cpd I with all choices of basis sets to within 1 kcal/mol. However, the R1/B1 barriers as well as HYD−RC and PC−RC gaps are increased by ca. 2 kcal/mol when full camphor is included in the QM region. The R1′/B1 barriers at R1/B1-optimized structures are 14.6/13.7/16.9/17.1 kcal/mol for 1 ^{3}A/2 ^{3}A/^{1}A/^{5}A states of Ox-Cpd I relative to 1 ^{3}A. When the basis set is extended to B2, the barrier (R1′/B2, 15.3/14.6/18.3/19.9 kcal/mol) is increased further by ca. 1 kcal/mol whereas PC is stabilized by ca. 4 kcal/mol relative to RC. The use of Wachters all electron basis set for iron further increases the barrier by ca. 2 kcal/mol (R1′/B2W, 17.3/16.4/19.8/18.2 kcal/mol) whereas PC is destabilized by ca. 4 kcal/mol, thus approaching the B1 result. With the extension of basis set from B1 or B2 to B2W, the HYD−RC gap on the ^{5}A surface is lowered by ca. 3 kcal/mol. These computational trends are valid for Cpd I/Cpd II/Ox-Cpd I, and our main conclusions thus do not change at our present best level R1′/B2W (barrier: 20.6/24.2/16.4 kcal/mol).

F. The Effect of Heme Environment. Our previous calculations[27,28] show that the inclusion of heme side chains in the QM region does not significantly change the QM/MM energetics for H-abstraction by Cpd I in $P450_{cam}$. When His355 and Asp297 are in the MM region,[27,28] the computed energetics are not affected by the choice of their protonation states, but for deprotonated Asp297 the A-prop environment is not consistent with the X-ray structure. The results with heme side chains, His355 and Asp297 included in the QM region[28] can be summarized as follows. When both Asp297 and His355 are protonated, there is no charge transfer involving propionates and their environments. When both His355 and Asp297 are deprotonated, one electron is transferred from Asp297 and A-prop to porphyrin, yielding Cpd II species with the formation of A-prop and Asp297 radicals. In this Cpd II species, the hydroxylation barrier is 3.6 kcal/mol higher than in the Cpd I species. This is in agreement with the present results in the absence of heme side chains and their environments in the QM region (R1′/B1 barriers: 21.9 [^{3}A] vs 17.8 kcal/mol [^{2}A], difference of 4.1 kcal/mol). When His355 is protonated but Asp297 is deprotonated, the A-prop environment is again inconsistent with the X-ray structure but the barrier is not affected. When Asp297 is protonated but His355 is deprotonated, a structure intermediate between Cpd I and Cpd II (spin density on both His355 and porphyrin: ca. 0.4e) is obtained with a slight barrier increase of 1.4 kcal/mol compared with the Cpd I species but with no electron transfer from the propionates and their environments.

In the remainder of this section, we investigate whether the electronic structures and energetics of Cpd II and Ox-Cpd I are affected by the choice of Asp297 and His355 protonation states when these residues are included in the QM region. The calculations employ the Prot2 protonation scheme and the B1 basis set.

1. Results for Cpd II. Single-point R2s calculations on R1/B1 Prot2 geometries of Cpd II with Asp297 and His355 in the QM region for the triplet ground state show that there is no spin density on the propionates, protonated Asp297 and His355, irrespective of the protonation state of His355 (barrier/endothermicity: 22.4/12.3 kcal/mol with protonated His355 and 22.6/11.9 kcal/mol with deprotonated His355, similar to the R1′/B1 result of 21.9/13.5 kcal/mol). For deprotonated Asp297, the oxygen atoms of A-prop and Asp297 carboxylates expel each other, yielding twisted A-prop and Asp297 side chains for both protonated (21.6/11.5 kcal/mol) and deprotonated (22.3/11.0 kcal/mol) His355 with no spin density accumulation on propionates and Asp297. Thus, protonated Asp297 is necessary for Cpd II to obtain geometries consistent with the X-ray structures, as in the case of Cpd I.[27,28] Cpd I is converted to Cpd II when Asp297 and His355 are deprotonated (see above) with electron transfer from Asp297.[27,28]

2. Results for Ox-Cpd I. R2s single-point calculations with protonated Asp297 and His355 on the R1/B1-optimized structures of triplet Ox-Cpd I demonstrate that there is no charge transfer between the heme side chains, Asp297, and His355, and the TS_H−RC/PC−RC gaps (15.8/−46.7 kcal/mol) are analogous to the R1′/B1 results (14.6/−45.3 kcal/mol). For the other combinations of protonation states of Asp297 and His355, single-point calculations indicate significant charge transfer involving these residues and propionates so that we performed geometry optimizations for these systems.

In the case of protonated Asp297 and deprotonated His355, the electron is ejected from His355 rather than porphyrin, yielding a spin density of ±1e on His355. Coupling between the unpaired electron on the His355 radical and the three unpaired electrons of Cpd I yields ^{5}A (^{3}A) [^{1}A] species with calculated barriers of 20.1 (19.1) [19.0] kcal/mol, which are analogous to those computed for Cpd I with closed-shell His355. In systems with deprotonated Asp297 (irrespective of the protonation state of His355), oxidation of Cpd I leads to a situation where one electron is shared between Asp297 and A-prop (spin density of ±0.6e and ±0.4e on Asp297 and A-prop; O−O distance of 2.2 Å between two carboxylates). Coupling with the three unpaired electrons of Cpd I again leads to ^{5}A (^{3}A) [^{1}A] species: in the case of deprotonated Asp297 and protonated His355, the corresponding calculated barriers of 20.0 (18.9) [18.9] kcal/mol are again consistent with those found for Cpd I in the absence of any charge transfer to propionates and their environments. Finally, in the case of deprotonated Asp297 and His355, there is significant electron transfer from His355 to porphyrin in the triplet state (spin densities on ^{3}A: A-prop, 0.42e; Asp297, 0.58e; His355, −0.54e), and the computed barrier of 19.7 kcal/mol appears again comparable with Cpd I.

G. Effect of Hartree−Fock Exchange. To check the sensitivity of our results toward the choice of hybrid functional, we have carried out B3LYP*/CHARMM calculations for the species studied in sections B−E (Figures 2−5). B3LYP tends to overestimate the stability of high-spin states of Fe(II) complexes,[59] and to correct for this deficiency the B3LYP* functional[59,60] has been introduced where the admixture of Hartree−Fock exchange has been reduced by 5% (from 20% to 15%). By design, high-spin species and systems with highly radicaloid character will be somewhat less stable in B3LYP* than in B3LYP. Single-point B3LYP*/CHARMM calculations (R1/B1) at B3LYP/CHARMM optimized geometries confirm this expected trend (see chapter 9 of Supporting Information for numerical results). In the reaction profiles for Cpd I (Figure 2), the relative energies of TS_H, HYD, and TS_R are increased by ca. 1, 3, and 1−2 kcal/mol, respectively. The relative energies of the pentaradicaloid species (Figure 3) are shifted upward by ca. 2−7 kcal/mol. In the reaction profiles for Cpd II (Figure 4), the barriers and endothermicities in the two lowest states rise by 1−2 and 3−4 kcal/mol, respectively. In the case of Ox-Cpd I (Figure 5), the relative energies are generally not affected not too much, with differences between B3LYP* and B3LYP of the order of 1 kcal/mol for RC, 1−3 kcal/mol for TSH, and 1 kcal/mol for HYD. Spin density distributions are generally similar in B3LYP* and B3LYP (see Supporting Information). B3LYP*/CHARMM geometry optimizations (R1/B1) have been performed only for the pentaradicaloid sextet state where the differences between B3LYP* and B3LYP energies are most pronounced: even in this case, the optimized geometries from B3LYP* and B3LYP are almost the same, and the reoptimization changes the relative B3LYP* energies by less than 0.5 kcal/mol (see Supporting Information).

In an overall assessment, the B3LYP*/CHARMM results thus confirm the qualitative conclusions drawn from the B3LYP/CHARMM calculations. They reinforce the central role of Cpd I in camphor hydroxylation, because the alternative pathways become even less favorable with B3LYP*/CHARMM. It should be emphasized that previous comparisons[17,32,37] have found B3LYP to be actually more reliable than B3LYP* for P450cam species, e.g., in reproducing the available experimental data on spin equilibrium (see ref 17 for a detailed discussion). The present B3LYP*/CHARMM calculations have thus only been done to check that the B3LYP/CHARMM results are not overly sensitive to the choice of hybrid functional, and this is indeed confirmed.

IV. Discussion and Conclusions

In this work, we have investigated camphor hydroxylation in $P450_{cam}$ for different electronic states of Cpd I and its one-electron reduced (Cpd II) and oxidized (Ox-Cpd I) forms. The calculations have been carried out at the QM/MM level using a new setup (snapX) that includes a catalytic water molecule w903 (H-bonded to the oxo atom of the moiety).[27,28]

The catalytic role of w903 was previously only studied for the quartet state. We now confirm that the presence of w903 also lowers the H-abstraction barrier in the doublet state by essentially the same amount and that the rebound step is not affected by w903. Hence, the two-state reactivity paradigm for $P450_{cam}$ hydroxylation remains valid also when including the catalytic water molecule.

As pointed out before,[16,17] pentaradicaloid quartet and sextet states of Cpd I can be generated from the triradicaloid ground states by one-electron excitation from the iron $d_{x^2-y^2}$ orbital to the d_{xy} orbital. The present QM/MM results for H-abstraction are analogous to those from a recent QM model study:[17] the pentaradicaloid states lie ca. 12 kcal/mol above the triradicaloid states in the case of Cpd I, but this energy difference diminishes along the reaction path by ca. 7 kcal/mol due to increased exchange interactions in the open-shell d block,[17] which leads to a substantial reduction of the H-abstraction barrier. This difference is expected to further decrease if zero point energy corrections are included,[17] and it is thus conceivable that pathways via pentaradicaloids may become competitive. We have also studied other excited states of Cpd I including a doublet with a spin flip on the iron d_{yz} orbital rather than the porphyrin a_{2u} orbital, which lies only 9 kcal/mol above the doublet ground state and has almost the same (low) barrier as the pentaradicaloid states. Single-point calculations indicate that excited states of Cpd I with Fe(V)−oxo character are high in energy (>20 kcal/mol); their reactivity could not be investigated due to SCF convergence problems (i.e., convergence to other, more stable solutions). We thus did not find any evidence that the postulated Fe(V)−oxo species[8] are mechanistically relevant.

One-electron reduction of Cpd I generates Cpd II which is computed to be ca. 90 kcal/mol more stable than Cpd I but shows sluggish reactivity, in agreement with previous experimental results.[24−26] The present QM/MM calculations yield H-abstraction barriers for Cpd II that are ca. 4 kcal/mol higher than those for Cpd I. One-electron oxidation of Cpd I requires ca. 170 kcal/mol to form Ox-Cpd I and should thus be very difficult to accomplish. The resulting tetraradicaloid Ox-Cpd I is more reactive than Cpd I, with H-abstraction barriers that are ca. 4 kcal/mol lower.

In continuation of our previous QM/MM studies of Cpd I,[27,28] we have also investigated the effects of different protonation states of Asp297 and His355 on Cpd II and Ox-Cpd I. The heme

(59) Reiher, M.; Salomon, O.; Hess, B. A. *Theor. Chem. Acc.* **2001**, *107*, 48.
(60) Salomon, O.; Reiher, M.; Hess, B. A. *J. Chem. Phys.* **2002**, *117*, 4729.

unit of Cpd II is not involved in any charge transfer with these environmental residues regardless of their protonation state. As in the case of Cpd I, an A-propionate environment consistent with the available X-ray structures is found for Cpd II only with protonated Asp297. Concerning Ox-Cpd I, there is no charge transfer involving Asp297 and His355 when they are both protonated (as in Cpd I). For the other protonation state combinations of Ox-Cpd I, the electronic structure of the heme unit corresponds to Cpd I or to a situation intermediate between Cpd I and Cpd II, and the computed H-abstraction barriers are generally similar to those for Cpd I. Taken together, our QM/MM results for Cpd I, Cpd II, and Ox-Cpd I show that the electron distribution in the region of the propionate side chains and the Asp297 and His355 residues can change to a considerable extent by redox events or upon protonation, but the effects on the H-abstraction barrier are always very minor.

In summary, the present study has broadened our view on Cpd I reactivity by considering different electronic states and oxidizing agents at the QM/MM level. The pentaradicaloid and some other excited states (such as the spin-flip doublet) have lower H-abstraction barriers than the triradicaloid ground state of Cpd I, around 10 kcal/mol or even less, and if formed, they are expected to be more reactive than Cpd I (provided that they do not relax faster to the ground state of Cpd I than they react). On the basis of the QM/MM results, other oxidizing agents seem less favorable: Cpd II (too sluggish), Ox-Cpd I (too costly to generate), and Fe(V)−oxo species (too unstable).

Acknowledgment. The research at Hebrew University was supported by a grant from BMBF (DIP-G.7.1).

Supporting Information Available: Detailed numerical results. This material is available free of charge via the Internet at http://pubs.acs.org.

JA066847Y